NRC Research Press

ARTICLE

Centrifuge experiments on the settlement of circular foundations on clay

B.T. McMahon and M.D. Bolton

Abstract: Centrifuge experiments were conducted to investigate the mechanisms governing the settlement of shallow circular foundations on clay. Model tests were performed on both soft and firm beds of overconsolidated kaolin clay. Foundation loads were applied as dead-weight and also through pneumatic loading. A Perspex window in the centrifuge package allowed digital images to be captured of a vertical cross section during and after the application of loading. Soil displacements deduced by particle image velocimetry (PIV) allow deformation mechanisms to be presented for undrained penetration, creep, and consolidation caused by transient flow. A technique is presented for discriminating consolidation settlements from the varying rates of short- and long-term creep. The mobilizable strength design (MSD) method is shown to make useful predictions of the undrained penetration using an estimated stress–strain behaviour of the clay with allowances made for anisotropy and rate effects. Subsequent creep and consolidation settlements were then determined using established correlations.

Key words: foundations, clay, settlement, undrained, consolidation, creep, centrifuge.

Résumé : Des essais en centrifugeuse ont été réalisés pour étudier les mécanismes gérant le tassement de fondations circulaires peu profondes sur de l'argile. Les essais modèles ont été réalisés sur des échantillons d'argile kaolin surconsolidés mou et fermes. Les charges de fondation ont été appliquées en tant que contrepoids, et par chargement pneumatique. Une fenêtre Perspex dans l'unité de centrifuge a permis d'obtenir des images digitales d'une coupe verticale durant et après l'application des charges. Les déplacements du sol déduits par la vélocimétrie par imagerie des particules (PIV) permettent de présenter les mécanismes de déformation pour la pénétration non drainée, le fluage et la consolidation due à l'écoulement transitoire. Une technique est présentée pour départager les tassements de consolidation des taux variables de fluage à court et long terme. L'article démontre que la conception de la résistance mobilisable (CRM) peut offrir des prédictions utiles de la pénétration non drainée à l'aide du comportement estimé en contrainte-déformation de l'argile avec des considérations pour l'anisotropie et les effets de taux. Le fluage et les tassements de consolidation subséquents ont ensuite été déterminés avec les corrélations établies. [Traduit par la Rédaction]

Mots-clés : fondations, argile, tassement, non drainé, consolidation, fluage, centrifugeuse.

Introduction

The rational design of spread foundations on clay is hampered by the lack of well-verified and straightforward settlement calculations. Theories of soil bearing capacity abound, but there is a comparative shortage of field observations of actual failures accompanying adequate ground investigation: a classical exception is the failure of the Transcona grain elevator (Baracos 1957). It has become clear, however, that in the case of more typical structures, damage begins to accumulate from quite small settlements of foundations, with the supporting soil being far from failure.

Analyses of the structural distortions and damage that can arise from differential settlement are becoming available, and general guidelines exist for various classes of structure. For example, settlement limitations for cylindrical steel storage tanks are discussed by Rosenberg and Journeaux (1982). A number of publications report settlements observed at full scale: an example is the settlement of cylindrical tanks reported by D'Orazio and Duncan (1987) and D'Orazio et al. (1989). If it were possible, therefore, to estimate the differential and total settlement of an oil tank on a raft foundation, it would be possible to check that it will be tolerable. Analyses exist for the ratio of differential settlement to average settlement both for rectangular and circular rafts of varying flexural stiffness carrying uniform surcharges from Horikoshi and Randolph (1997). So the extension of rational displacement-based design criteria to more general spread foundations can also be contemplated. An equivalent full scale application for the model tests and calculations reported herein would be a fluid storage tank on a stiff raft foundation, subjected to quick filling and prolonged observations of settlement. The most significant obstacle is the practical estimation of an appropriate nonlinear soil stiffness, with any necessary allowances for anisotropy and rate effects. That is the goal of this paper.

The nonlinearity of soils has generally meant that settlements have either been estimated using the elasticity theory with an empirical value of elastic modulus, or through nonlinear finite element analysis. Neither alternative is optimal for decision making. This paper demonstrates the use of relatively straightforward bearing capacity and nonlinear settlement calculations in relation to centrifuge model tests of rigid circular foundations on clay.

Conventional calculations

A mechanism to determine bearing capacity was first investigated by Prandtl (1921) using plasticity theory on metals. Elastic strains were assumed to be small compared with plastic strains, and both anisotropy and rate effects were ignored. Terzaghi (1943) applied Prandtl's findings to shallow foundations on soils. Later

Received 14 May 2013. Accepted 11 January 2014.

B.T. McMahon and M.D. Bolton. Department of Engineering, University of Cambridge, Schofield Centre, High Cross, Madingley Road, Cambridge, CB3 0EL, UK.

Corresponding author: B.T. McMahon (e-mail: b.mcmahon84@gmail.com).

Published at www.nrcresearchpress.com/cgj on 11 February 2014.

Cox et al. (1961) and Eason and Shield (1960) used rate-independent plasticity theory to estimate the bearing capacity factors (ultimate bearing pressure normalized by soil shear strength) of smooth and rough circular shallow foundations on undrained clay as N_c = 5.69 and 6.05, respectively. Foundation designers use such results to determine the theoretical bearing capacity of spread foundations, and then divide it by some "factor of safety" (typically 2.5 to 3) to derive an allowable working load. This large reduction factor is sometimes justified on the basis of uncertainty in soil properties. The avoidance of structural damage also makes it necessary to control settlements, and this must also lead the designer to employ lower bearing pressures.

The conventional calculation of the total settlement of a foundation, w_t, regards it as the sum of "primary" and "secondary" components. The primary settlement is thought to be composed of the immediate undrained component, w_u, and the consolidation component, w_c, due to drainage, while the secondary settlement, w_s, is attributed to creep. The total settlement is

$$w_t = w_u + w_c + w_s \tag{1}$$

A number of methods exist for determining the components of primary settlement, typically based on isotropic elasticity. For example, Davis and Selvadurai (1996) show that the settlement of a rigid circular punch of diameter, D, carrying an average contact pressure, q, over a deep, homogeneous elastic bed with Poisson's ratio, ν, and shear modulus, G, can be written as

$$w = \frac{\pi}{8}\frac{(1-\nu)}{G}qD \tag{2}$$

The shear modulus, G, has a unique value irrespective of drainage conditions. The immediate settlement w_u is undrained, occurring at constant volume, and therefore the undrained Poisson's ratio ν_u = 0.5 is used. The primary settlement ($w_u + w_c$) also includes the dissipation of excess pore pressures, so effective stresses change and the parameter ν' must be adopted.

Equation (2) can then be used to deduce the ratio of the final consolidation settlement to the initial undrained penetration

$$\frac{w_c}{w_u} = (1 - 2\nu') \tag{3}$$

Values of G and ν' for clays are highly dependent on strain magnitude, and can also display significant anisotropy. Poisson's ratio can be very small when measured over very small strain excursions in overconsolidated clay; for example, Gasparre (2005) found typical values of $\nu'_{hh} \approx -0.03$, $\nu'_{vh} \approx +0.05$ for high-quality cores of London clay. Secant values of ν' in lightly overconsolidated clay deduced from changes in K_0 observed in stress path triaxial tests with significant unloading and reloading were reported (Wroth 1975) to be larger, typically falling between 0.25 and 0.35. As heavily overconsolidated clay ultimately tends to dilate as it approaches peak strength, its secant ν' must reach 0.5 at some intermediate strain when the net volume change passes through zero. As the magnitude of a strain excursion increases it becomes largely irrecoverable, of course, and a strain-hardening elastic–plastic formulation for stress–strain would be preferred. The current paper will demonstrate that the calculation of tolerable settlements for shallow foundations on overconsolidated clays may be estimated using a modified elastic approach with a secant value of $\nu' \approx 0.25$ to 0.5.

The secondary settlement results from soil particle rearrangement under constant effective stress. Methods exist for determining the creep settlement, with a common approach utilizing the secondary compression index $C_{\alpha\varepsilon}$ obtained from a plot of extended strain versus the logarithm of time in an oedometer test. If every component of primary soil strain can be assumed to increase with the logarithm of time at a rate $C_{\alpha\varepsilon}$, it would follow that primary settlement would extend similarly, so that secondary settlements could be predicted. The creep settlement of clays and sands should then appear insignificant compared to the primary settlement, as Skempton and Bjerrum (1957) remarked in a footnote. However, this was not the case for large storage tanks on clay reported by Foott and Ladd (1981); they inferred very significant creep settlements but could not suggest a straightforward calculation procedure. This problem remains.

Simplified nonlinear analysis

Any improvement in conventional settlement calculations must begin with a better representation of the actual soil deformation mechanisms, and by accounting for nonlinear and rate-dependent soil stress–strain behaviour. The mobilizable strength design (MSD) method, as adapted to circular shallow foundations by Osman and Bolton (2005), offers a way of accounting for soil nonlinearity by scaling a triaxial stress–strain curve to make direct predictions of foundation load–settlement behaviour. An undrained soil deformation mechanism was assumed within the boundaries of the classical plane–strain Prandtl bearing capacity mechanism. Although the solution avoided the use of any slip lines, it was shown through an overall energy balance that the average shear stress mobilized within the mechanism was related to the current bearing stress q by approximately the same bearing capacity factor N_c currently employed at failure

$$\tau_{mob} = \frac{q}{N_c} \tag{4}$$

The average strain γ within that mechanism was related to the undrained settlement w_u

$$\gamma = \frac{M_c w_u}{D} \tag{5}$$

where M_c is a compatibility factor equal to 1.35. Equations (4) and (5) provide the scaling from a simple soil test curve of (τ, γ) to a loading curve (q, w_u).

Osman and Bolton (2005) went on to corroborate MSD using nonlinear finite element analysis based on a rate-independent nonlinear stress–strain relation. Undrained load settlement curves for a foundation on clay whose strength increased with depth were found to be effectively identical when the MSD prediction was made using stress–strain data from a depth 0.3D below the interface. The centrifuge experiments described below were performed with the aim of checking the applicability of this undrained MSD mechanism and of demonstrating necessary allowances for strain-rate, consolidation, and creep effects.

Centrifuge testing

A series of centrifuge experiments was performed on the Cambridge 10 m diameter beam centrifuge, to investigate shallow circular foundations on clay tested at a nominal 100*g* imposed at the clay surface.

Centrifuge package

The centrifuge strong package consisted of an aluminium U-frame, steel back plate, and Perspex window. The internal dimensions were 790 mm × 200 mm × 560 mm deep. To reduce friction, the interior metal surfaces were plated with polished hard chrome and the Perspex window was greased. Semicircular foundations were chosen to facilitate analysis in axial symmetry. Digital cameras were used to capture images at all stages of loading.

This allowed soil deformations to be calculated using particle image velocimetry (PIV) (White et al. 2003). Observations confirmed that three foundations could be tested simultaneously with sufficient spacing to avoid cross-interference.

Foundation loads

One-dimensional actuators were developed to apply foundation loads to the soil body as outlined in McMahon and Bolton (2011). One foundation in each test was rigidly connected to a pneumatic cylinder, allowing incremental loads to be applied using compressed air. The initial load was applied through the dead-weight of the combination of an 11 mm thick aluminium base, its connecting rod, and the pneumatic cylinder piston, resulting in a mean bearing pressure of about 72 kPa. Compressed air was applied to the top inlet of the pneumatic cylinder for subsequent load increases. The resulting pressures on the soil were 140 and 280 kPa. The remaining two foundations simply applied a load to the soil through their dead-weight, with 40 mm thick bases providing a mean bearing pressure of about 100 kPa. All model foundations could be described as effectively rigid in the tests.

Compressed air was applied to the bottom inlet of the pneumatic cylinders to suspend the foundations above the clay surface during spin-up and clay consolidation. When consolidation was judged to be sufficiently complete, the compressed air was slowly reduced, allowing the base to fall gently onto the surface under its own self-weight. Each foundation was loaded independently, approximately 15 min apart.

Instrumentation

Lasers were mounted to measure the settlement of each foundation and validate PIV results. Pore pressure transducers (PPTs) were placed below each foundation at a depth of about one half of the base diameter beneath the centre and the edge, with an additional PPT at the quarter-line beneath the 100 mm diameter bases. A PPT was also placed in the standpipe that controlled the elevation of the water table. Load cells were placed above the foundations to verify the load being applied and to monitor the friction (if any) between the foundation and the Perspex window. A schematic of the experiment set up is shown in Fig. 1.

Model preparation

A base drain was created by pouring a dense layer of fine sand to a depth of 30 mm in the package before saturating it through the bottom drainage inlets. Polwhite E-grade kaolin clay powder was mixed under vacuum at a water content of 100%, and the clay slurry was carefully placed (to prevent air bubbles) onto the drainage layer. The model was then placed in a computer-controlled consolidometer and load was applied to the clay via a piston–approximately doubling the load every three days (once excess pore pressures had dissipated) up to the final pressures of 140 kPa for the soft clay models and 500 kPa for the firm clay models. PPTs were inserted in augered holes and backfilled with slurry, prior to the final stage of consolidation. When all excess pore pressures had dissipated, the model was unloaded in increments of no more than 80 kPa, allowing the clay to swell each time to prevent cavitation. However, the final unloading step from 60 to 0 kPa was performed without allowing any water to enter the clay, thereby maintaining effective stress whilst avoiding air entry.

The surface of the clay was trimmed and levelled and the front face treated by gently blowing coloured sand on to it to provide texture for PIV analysis. The front of each base was also painted for texture. The Perspex was lubricated to reduce friction on the base and the soil. Then the package was assembled.

Test procedure

Spin-up of the centrifuge was performed in 20*g* increments up to the testing level of 100g. A constant water supply was provided to the clay through a standpipe with an overflow coinciding with the clay surface, thus maintaining the water table at that level. Consolidation progress was monitored through the pore pressure transducers in the model and the standpipe. The foundation loads were only applied after approximately 3 h, when self-weight consolidation was substantially complete. Figure 2 shows the pore pressures recorded by a PPT at a depth of 55 mm below the loading area of a 100 mm diameter base. The initially negative value (u = −30 kPa) corresponds to the initial state of effective stress in the soil prior to centrifuging. The stepped increase to u = 85 kPa corresponds to centrifuge spin-up, and the subsequent reduction over the next 3.5 h corresponds to self-weight consolidation. The test was suspended briefly to correct a camera issue. The model was spun-up again and allowed to consolidate for 1 h before the foundation was gently lowered with the pore pressure responding accordingly, and then dissipating once again. This was repeated twice more in subsequent loading stages effected by the compressed air piston. Figure 2 shows that full self-weight consolidation was only achieved after about 8 h and therefore base loads had to be applied with some remaining excess pore pressure still present. More details can be found in McMahon (2012).

Digital cameras were controlled through the use of PSRemote©. Before applying load, the time interval between photographs was set as 5 s during the early undrained phase and 30 s during the later stages of the test. Three centrifuge models were conducted with clay, with a total of seven tests providing load settlement time data. Table 1 offers a summary of the tests, indicating the preconsolidation pressure, the base diameter, and both the time to apply the load to the soil and the load test duration.

The testing procedure did not include in flight soil testing. Although T-bar tests might have been used, there remains significant uncertainty regarding the calibration that should be used at shallow depth, prior to the development of a full flow around mechanism. White et al. (2010) use large deformation finite element analysis to derive a shallow correction factor, although the analyses are based on uniform soil beds whereas a strong increase in undrained strength with depth would be apparent in the heavily overconsolidated kaolin beds in the present study. Considering this source of uncertainty and the need to obtain soil deformability data, an alternative strategy for soil testing was adopted. A parallel programme of triaxial testing was carried out (Vardanega et al. 2012) on the kaolin following a variety of stress histories similar to those applying at different depths in the centrifuge models. These tests will be used below to estimate soil strength and deformability at the shallow depths that are representative of soil deformations below the foundations.

Results and discussion

Results observed across all foundations and clay models showed consistent trends in behaviour. The detailed results for one foundation on stiff clay are provided as an indicator of self-consistency. This is followed by an analysis and discussion based on key results from all the tests.

Consistency of settlement measurements

Applying load through dead-weight is analogous to fast loading by filling an oil or water storage tank. The advantage is that clear mechanisms were observable in the centrifuge over the whole timescale, from 1 s (3 h at prototype scale) up to 6 h (7 years at prototype scale). The pneumatic actuator could offer further stages of loading. A camera with higher resolution was used for the stiff clay (test 3), providing more detailed images and better results from PIV. These higher resolution images, for a pneumatically loaded 100 mm diameter base, are therefore used as an exemplar below (see test 3A in Table 1). A comparison between PIV and laser data are included in Fig. 3, showing excellent agreement. Only movements recorded by the lasers will subsequently be presented, indicating the settlement of the foundation relative to the ground in the far field.

Fig. 1. Schematic diagram of centrifuge package.

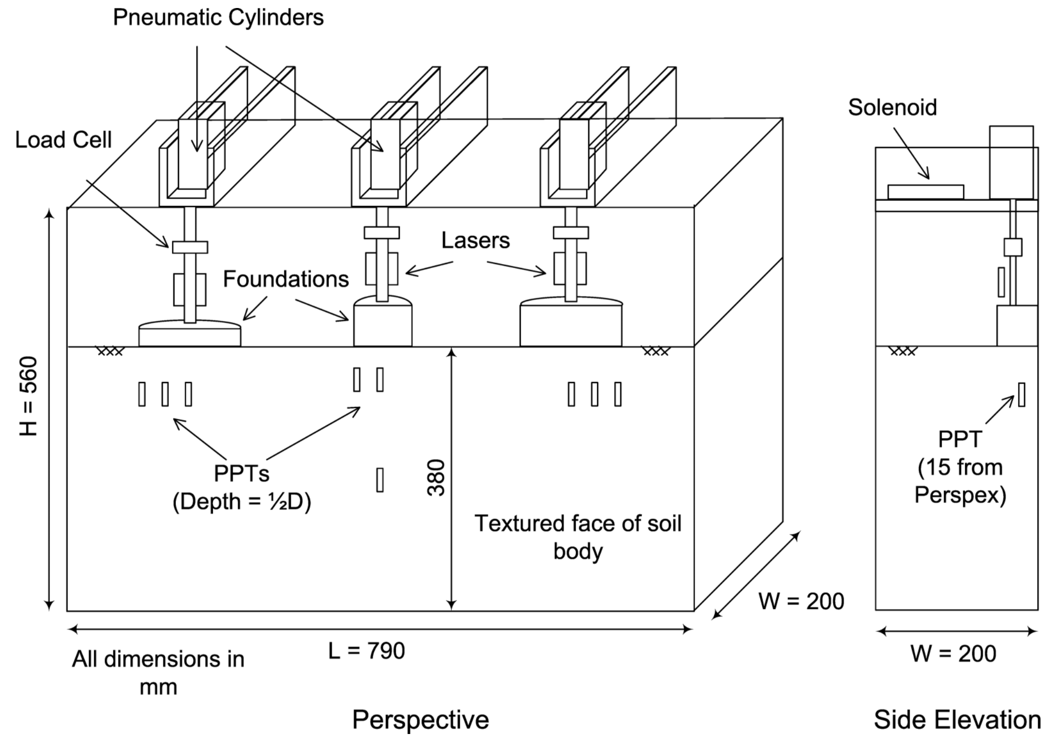

Fig. 2. Pore pressure distribution for entire duration of test 3A.

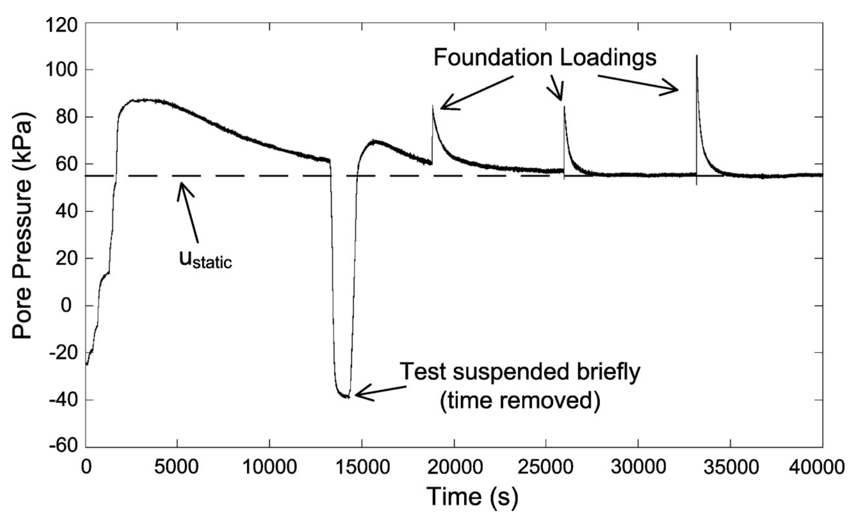

Table 1. Summary of centrifuge tests showing foundation diameter, average load, and relevant timings.

Test	$\sigma'_{v,max}$ (kPa)	D (mm)	Load (kPa)	Time to apply load (s)	Total load duration (h)	Test label
1	140	50	100	0.5	5	1A
		50	117	2	0.01	1B
2	500	50	100	2	1	2A
		100	100	6	1	2B
3	500	100	72	7	2	3A
		50	100	5	6	3B
		100	100	11	6	3C

Undrained penetration in test 3A

The immediate response of a saturated soil to a load is to resist volume change, with settlement occurring through shear. Excess pore pressures beneath the base can be used to record drainage effects. Figure 3 portrays measurements for the first 100 s of testing in test 3A. The load cell data shows that the average pressure ultimately applied to the soil was approximately 72 kPa. As a consequence of reducing the compressed air pressure that was holding the foundation suspended, the base was gently lowered so that its full load took approximately 7 s to apply (time t_0). By weighing the loading components before the experiment this load magnitude was independently estimated, indicating that any friction between the foundation and the Perspex interface was negligible. Figure 3 also portrays the foundation movement and associated excess pore pressure measured beneath the centreline at a depth of 0.55D.

An undrained penetration of 0.82 mm occurred once the full load was applied and this generated an excess pore pressure of about 25 kPa. The excess pore pressure on the centreline can then be seen to rise to approximately 27 kPa. An increase of this sort

Fig. 3. Plot of average foundation load, movement, and excess pore pressure on foundation centreline for first 100 s in test 3A.

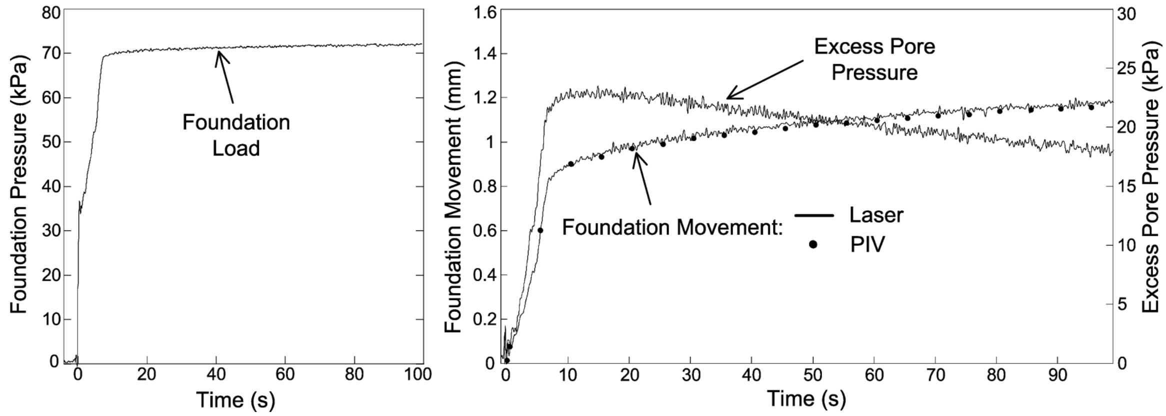

was seen in all of the tests and can be attributed to load redistribution because of peripheral drainage (Mandel 1953). Because transient drainage occurs more rapidly at the edge of the load, the soil beneath the edge would settle faster if the load were flexible. In the case of a rigid base, or in Mandel's analysis of a stiff embankment on a soft soil, the effect is to redistribute load from the edges towards the centre. This causes additional excess pore pressure beneath the centre. Schiffman et al. (1969) referred to this general phenomenon as the Mandel-Cryer effect. The load redistribution phase appears to take place as soon as the load has been fully applied, at time $t_0 \approx 7$ s in Fig. 3, but more regional dissipation of pore pressure affecting the central PPT at a depth 0.55D only became obvious after time $t_1 = 10.5$ s.

A PIV analysis was performed on an area of soil beneath the foundation at time $t_1 = 10.5$ s. The soil movement immediately beneath the base is about 0.86 mm — as also observed by the laser data of settlement in Fig. 3. Figure 4 shows relatively small horizontal movements of the soil in contact with the base, consistent with a moderately rough interface. There is not much adjacent heave, and the mechanism resembles cavity expansion more than rigid plastic indentation: this was developed as a new bearing capacity and settlement calculation by McMahon et al. (2013). The mechanism in Fig. 4 was found to be of constant volume except for the small region immediately below the edge where the singularity prevents the accurate estimation of volume changes.

Fig. 4. Mechanism at time t_1 (10.5 s) for 100 mm diameter foundation on stiff clay in test 3A.

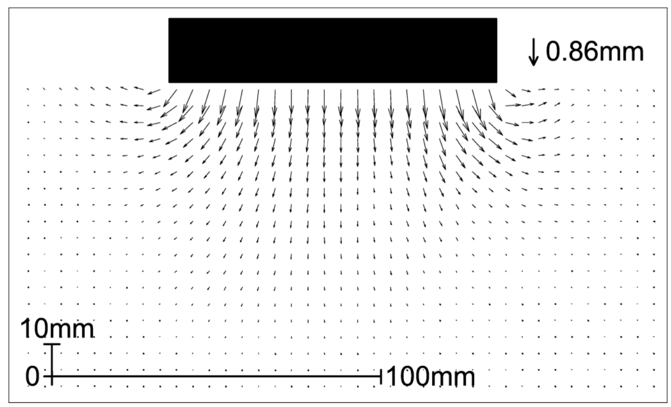

Fig. 5. Comparison of mechanism between undrained penetration (t_1) and during creep and consolidation phase (t_2) in test 3A.

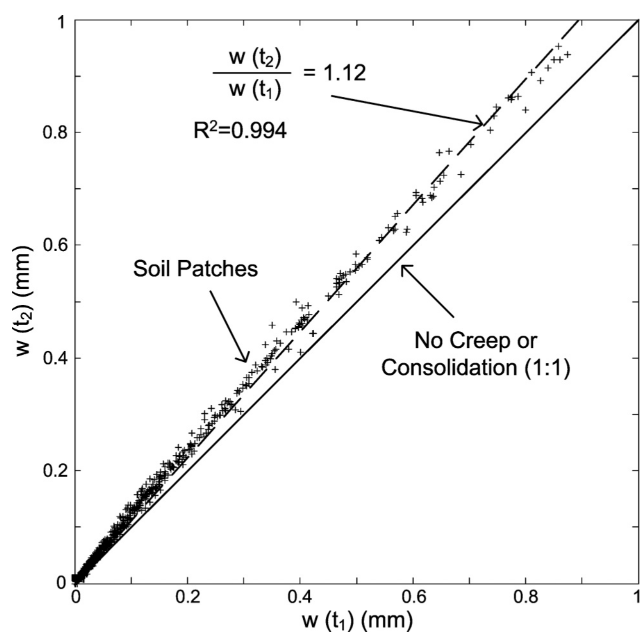

Consolidation and creep in test 3A

The settlement between t_1 and t_2 (about 30 s after loading) occurs with the excess pore pressure at 0.55D beneath the centre, dropping 4% from its peak. The settlement during this period may be attributed to the following mechanisms:

1. Local drainage of the soil under the edge of the foundation, coupled with added total stress being carried under the centre, leading to additional undrained penetration.
2. General creep following the shear mechanism induced by base penetration.

The PIV results portrayed much the same mechanism at time t_2 as the undrained penetration shown in Fig. 4, but with each soil patch vector simply amplified by a common factor. Figure 5 demonstrates that these movements were multiplied by a factor of 1.12 on average. So the combination of mechanisms 1 and 2 contributed an additional settlement equal to 12% of the undrained penetration during this time period, a rate of 26% for a factor of 10 on time.

The settlement and excess pore pressures for the whole 2 h loading stage are shown in Fig. 6. It can be seen that excess pore pressures had substantially dissipated after approximately 4000 s (time t_3). The pore pressure then continues to fall to a value of about −2 kPa. This is attributable to the initial excess pore pressure after self-weight consolidation (shown in Fig. 2), which had been taken as datum during the loading event. A deformation mechanism for consolidation and creep occurring between times of 140 and 600 s is presented in Fig. 7. The magnitude of movement beneath the foundation is approximately 0.25 mm during

Fig. 6. Foundation movement and excess pore pressure for the first loading phase in test 3A.

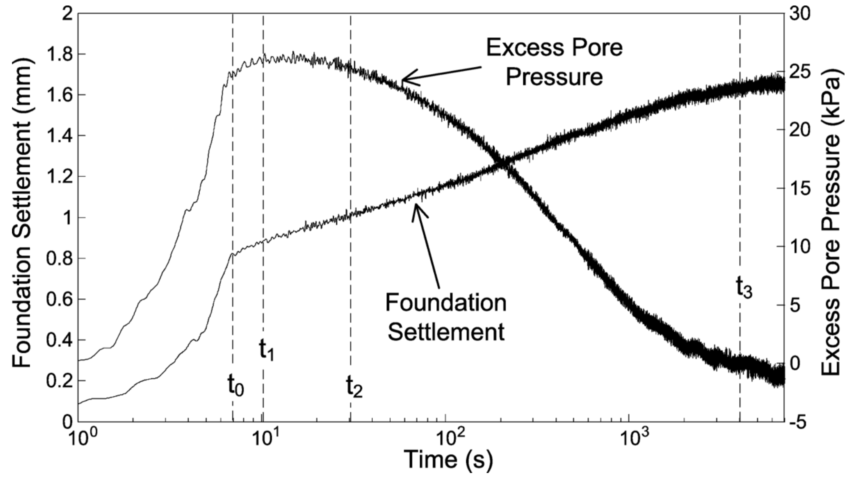

Fig. 7. Consolidation and creep mechanism between times of 140 and 600 s in test 3A.

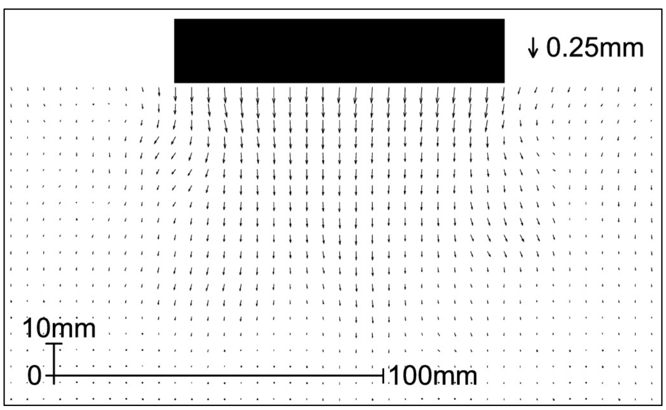

this time. The mechanism demonstrates a quasi one-dimensional compression of soil beneath the base between these times.

Continued settlement seen in Fig. 6 more than 4000 s after loading, after excess pore pressures have substantially dissipated, indicates drained creep of the soil due to the foundation load. Other tests enjoyed longer drained creep periods, but the corresponding deformation mechanism could not be constructed because of the relatively small magnitude of movement and "noise" in the PIV data.

Back-analysis

Previously published data on the strength and stiffness of clays is first used to estimate the bearing capacity of a 50 mm diameter base on the soft clay in test 1B, for comparison with the measured value. Having demonstrated an acceptable match, the same relationships are used to back analyze the undrained load-penetration data. A model for consolidation and creep is then proposed.

Bearing capacity test on soft clay

Ladd et al. (1977) investigated the effect of the degree of overconsolidation on the undrained shear strength of clays and found

$$\frac{c_u}{\sigma'_{v,0}} = \left(\frac{c_u}{\sigma'_{v,0}}\right)_{nc} (\mathrm{OCR})^{\Lambda} \tag{6}$$

where c_u is the undrained shear strength, $\sigma'_{v,0}$ is the vertical effective stress, nc denotes normally consolidated, OCR is the overconsolidation ratio, and Λ is regarded as an empirical exponent that apparently reduces from 0.85 to 0.75 with increasing overconsolidation, but is taken here as 0.8. For the kaolin used in these tests, Vardanega et al. (2012) quote a value of $(c_u/\sigma'_{v,0})_{nc} = 0.23$ pertinent to triaxial compression tests carried out at an axial strain rate of 1.2%/h, which corresponds to a shear strain rate of 5.0×10^{-6} s^{-1}. As with the nonlinear FEA validations used by Osman and Bolton (2005), the soil properties for back-analysis will pertain to a characteristic depth of $z = 0.3D$.

The clay in test 1 was consolidated to 140 kPa before centrifuging. Therefore, for the 50 mm diameter base in test 1B the characteristic depth is 15 mm, offering an in situ stress $\sigma'_{v,0} = 11.7$ kPa, with OCR = 12, and $c_u = 20$ kPa from eq. (6). Comparative data for all the tests is given in Table 2. The undrained mechanism of Fig. 4 shows that the base is relatively rough and therefore a bearing capacity factor of $N_c = 6.05$ is adopted. This produces a theoretical net bearing capacity of $q_{ult} = 121$ kPa, based on triaxial compression data.

Figure 8*a* demonstrates the configuration of the load cell used during the experiment and shows how the load cell readings were interpreted. Figure 8*b* presents the results from the bearing capacity test 1B and indicates an average bearing capacity of $q_{ult} =$ 117 kPa, which compares extremely well with the predicted value. This may be fortuitous, however, because the effects of embedment, anisotropy, and strain rate have so far been neglected. The bearing pressure of 117 kPa is seen in Fig. 8*b* to be acting after only 2 s, when the settlement is about 12 mm. At this depth of embedment the overburden pressure is 20 kPa, so the net bearing pressure is about 97 kPa. This corresponds to an average shear strain estimated from eq. (5) of $1.35 \times 12 / 50 = 32.4\%$, which is far beyond the point of peak strength recorded in the triaxial tests on the same soil reported by Vardanega et al. (2012). These tests typically exhibited 30% softening at a gross overall shear strain of 15%, although it must be recognized that the actual magnitude of strain and the degree of softening are a function of localization whose severity depends on deformation constraints.

If, notwithstanding, the shear strain rate during the bearing failure is taken as 0.162 s^{-1}, that is about 3×10^4 times faster than the triaxial tests that were used to estimate c_u. Kulhawy and Mayne (1990) demonstrated a correlation between undrained strength and strain rate for 209 undrained triaxial tests on a total of 26 clays

$$\frac{c_u}{c_{u,0}} = \left[1 + 0.1 \log_{10}\left(\frac{\dot{\gamma}}{\dot{\gamma}_0}\right)\right] \tag{7}$$

Table 2. Soil properties inferred at $z = 0.3D$, and the undrained settlement predicted using MSD.

	Soil properties inferred at $z = 0.3D$									
Test label	z (mm)	$\sigma'_{v,0}$ (kPa)	OCR	c_u (kPa)	$\gamma_{M=2}$	$\dot{\gamma}$ (s^{-1})	$c_{u,mod}$ (kPa)	$\tau_{mob}/c_{u,mod}$	γ	$w_{u,pred}$ (mm)
1A	15	11.7	12	20	0.022	0.1226	22	0.76	0.044	1.62
1B	15	11.7	12	20	0.022	0.1620	22	—	—	—
2A	15	12.2	42	55	0.050	0.0136	57	0.29	0.020	0.76
2B	30	24.3	21	63	0.031	0.0018	61	0.27	0.011	0.84
3A	30	24.0	21	63	0.031	0.0009	59	0.20	0.007	0.51
3B	15	12.0	42	55	0.050	0.0055	55	0.30	0.022	0.81
3C	30	24.0	21	63	0.031	0.0010	59	0.28	0.012	0.88

Fig. 8. Bearing capacity test information: (*a*) load cell readings during foundation suspension and base loading and (*b*) foundation settlement and bearing pressure of bearing capacity test 1B.

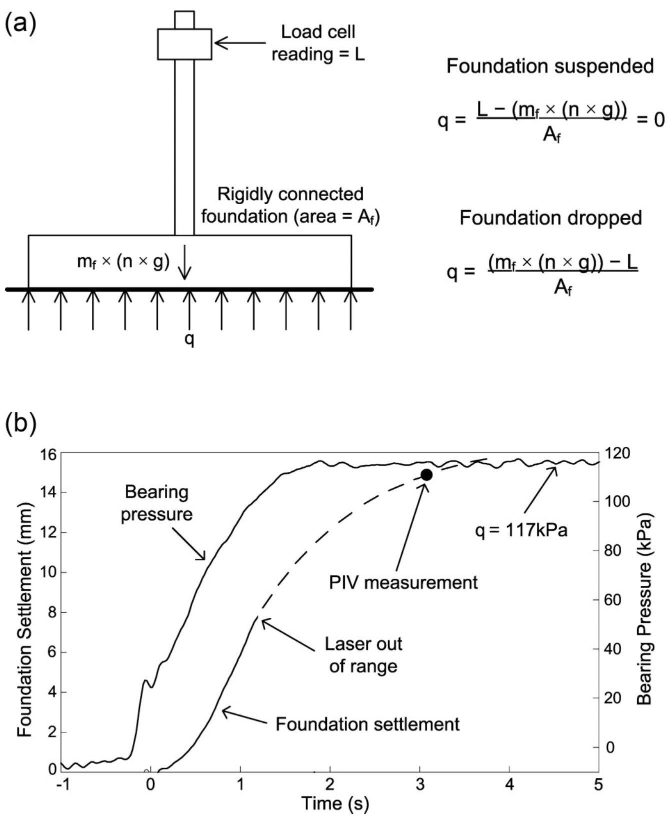

This would suggest that the clay strength in test 1B should be increased by a factor of 1.45, giving a theoretical net bearing capacity of 175 kPa.

However, some allowance should also be made for anisotropy. Kulhawy and Mayne (1990) demonstrated that for kaolin with a plasticity index of 33%, the ratio of undrained strength in triaxial tests in extension and compression typically falls in the range of 0.55 ± 0.15. Furthermore, Osman and Bolton (2005) demonstrated that the field loading tests of a 2 m square footing on soft silt reported by Lehane (2003) were approximately consistent with the average of the strengths measured for cores in compression and extension. It might therefore be expected that the ratio of the operational strength in a bearing capacity problem and the shear strength in triaxial compression would be about 0.77. Applying this to the previous estimate of 175 kPa for the fast penetration of the foundation, the estimated bearing capacity reduces to 135 kPa. This is 39% higher than the observed net bearing pressure applied in the test, which is taken to signify 39% post-peak softening, similar to that observed in the triaxial tests reported by Vardanega et al. (2012) at similarly large strains. This back analysis of the fast bearing capacity test 1B must be regarded as broadly satisfactory, although it is noted that the corrections for strain rate, anisotropy, and post-peak softening almost exactly cancel each other.

Undrained settlement

Vardanega et al. (2012) report triaxial compression test data for the same batch of kaolin used in the centrifuge tests, and fitted a nonlinear stress–strain model:

$$\tau_{mob}/c_u = 0.5\,(\gamma/\gamma_{M=2})^b \text{ in the range } 0.2 < \tau_{mob}/c_u < 0.8 \tag{8}$$

with eq. (9) for the exponent b and eq. (10) for the mobilization strain $\gamma_{M=2}$ varying as functions of overconsolidation ratio (OCR) in the range 1 to 20

$$b = 0.011(\mathrm{OCR}) + 0.371 \tag{9}$$

$$\gamma_{M=2} = 0.0040(\mathrm{OCR})^{0.68} \tag{10}$$

Vardanega and Bolton (2011, 2012) had previously shown that eq. (8) offered a good fit to the stress–strain data of a wide variety of natural clay soils, with $b = 0.6$ as an overall regression. In the absence of any data for kaolin at OCR > 20, a value of $b = 0.6$ has been used for all subsequent calculations, corresponding to OCR ≈ 21 in eq. (9). Values of nominal undrained strength and nonlinear stiffness for the kaolin clay, with a stress history equivalent to any desired depth in the centrifuge model, can then be inferred using eqs. (6), (8), and (10). These values can subsequently be corrected for embedment, rate, and anisotropy effects, as explained earlier.

The firm clay of test 3 was consolidated to a pressure of $\sigma'_{v,max}$ = 500 kPa. Figure 9 shows the corresponding profiles of stress, overconsolidation ratio, and nominal strength, together with the location of the characteristic depth of 30 mm in test 3A. At this depth, OCR = 21, c_u = 63 kPa, and $\gamma_{M=2}$ = 0.031. The nominal stress–strain curve deduced from eq. (8) is given in Fig. 10 and this will be modified for use in MSD calculations of settlement in the tests.

The mobilized shear stress in the soil beneath foundation 3A is determined as $\tau_{mob} = q/N_c = 72/6.05 = 12$ kPa. This was the least heavily loaded of the model foundations. The nominal degree of mobilization ($\tau_{mob}/c_u = 0.19$) is just below the validated range for eq. 8. This is indicated on the stress–strain curve of Fig. 10 and corresponds to a nominal shear strain $\gamma = 6.3 \times 10^{-3}$. The average shear strain-rate during undrained loading can now be computed as 9×10^{-4} s^{-1} using the information that it took 7 s for the load to be fully applied. This is 180 times faster than the triaxial tests, so eq. (7), found from the strain rate data both above and below this value, implies that the undrained strength would have been enhanced by a factor of $1 + 0.1 \log_{10}180 = 1.23$ had it been fully mobilized.

The operational strength accounting for anisotropy should be reduced by a factor of 0.77, as discussed above. Embedment is

Fig. 9. Profile of in situ and preconsolidation stress, overconsolidation ratio, undrained shear strength, and mobilization strain with depth for test 3A.

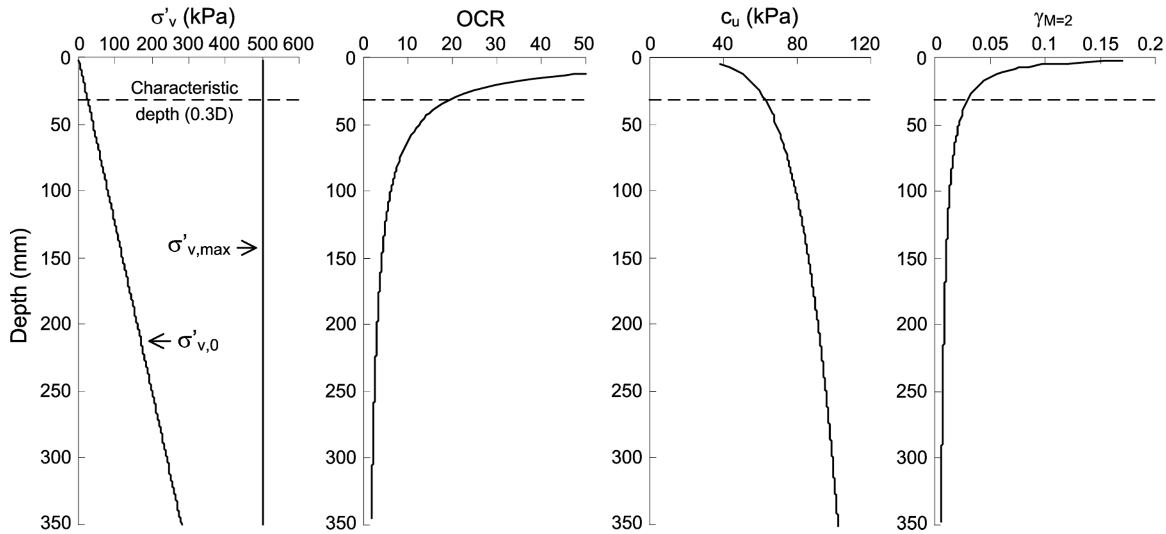

Fig. 10. Stress–strain curve at characteristic depth of 0.3*D* using the kaolin database of Vardanega et al. (2012).

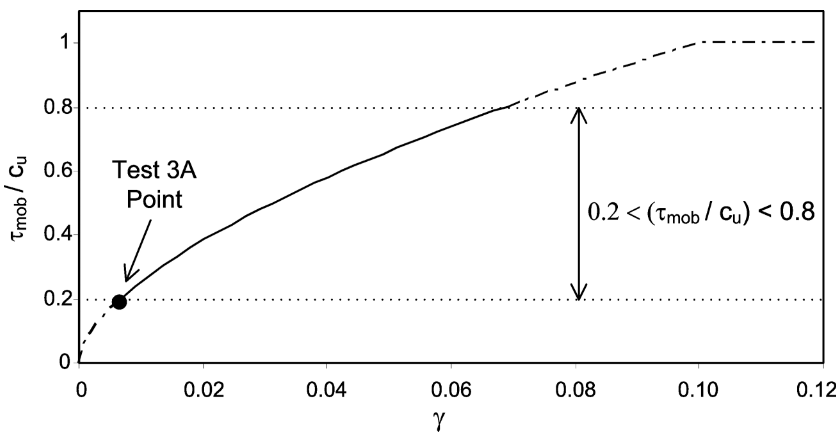

negligible in this case, and in the remaining settlement tests, so no allowance for overburden or softening is appropriate. The net reduction in the estimated shear strength in bearing is therefore by a factor of 0.94. Introducing this correction into eq. (8) the mobilization increases to $\tau_{mob}/c_{u,mod}$ = 0.20 and the estimated shear strain rises to 6.9×10^{-3}.

The calculated undrained settlement in test 3A is, therefore, 0.51 mm compared to the observed settlement of 0.82 mm, 7 s after the load was applied. Although the discrepancy may appear alarming when expressed as a factor error of 1.6, this is the largest encountered in the back analyses, pertaining to the foundation with the smallest settlement (and the largest factor of safety).

Table 2 shows the nominal soil properties for each test and their predicted undrained settlements, $w_{u,pred}$. Figure 11 shows the predicted undrained settlement plotted against the experimental settlement $w_{u,exp}$ at the time of first application of the full load. The measurements are typically 0.2 mm larger than the predictions, which might relate to a lack of perfect fit at the foundation interface. Even if the discrepancy corresponds to genuine calculation errors it might be regarded as tolerable considering the multiplicity of real world challenges — a nonlinear strength profile with depth, nonlinear stiffness, rate, and anisotropy effects.

Time effects

According to both Lin and Wang (1998) and Kwok and Bolton (2010), the creep of soils for moderate degrees of shear stress mobilization can be expressed as

Fig. 11. Predicted undrained settlement plotted against experimental undrained settlement.

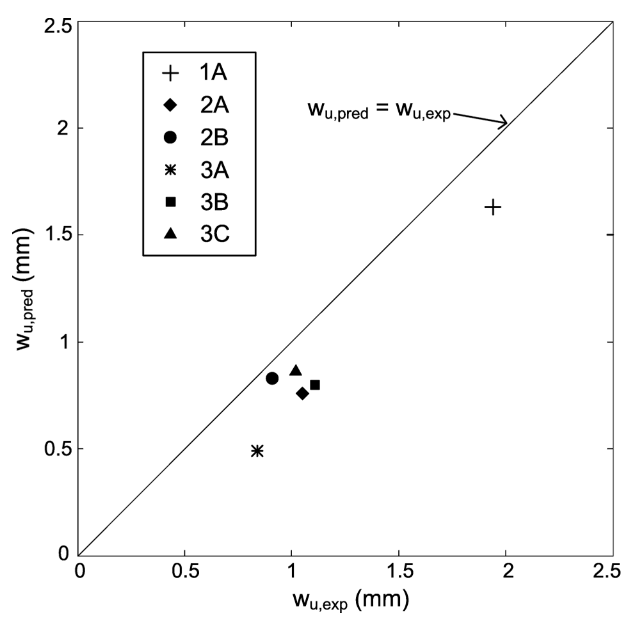

Fig. 12. Model developed to determine creep and consolidation settlements.

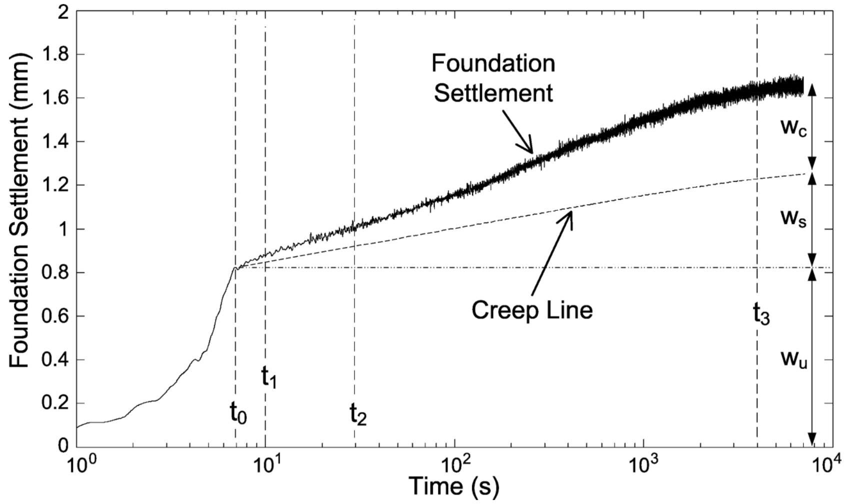

$$\gamma = \gamma_0\left(\frac{t}{t_0}\right)^{\alpha} \tag{11}$$

For relatively small creep strains $\Delta\gamma \ll \gamma_0$ eq. (11) can be written

$$\frac{\Delta\gamma}{\gamma_0} = \alpha \ln\left(\frac{t}{t_0}\right) = 2.3\alpha \log_{10}\left(\frac{t}{t_0}\right) = C_{\alpha\gamma} \log_{10}\left(\frac{t}{t_0}\right) \tag{12}$$

which accords with the usual symbolic form for secondary strains, except that symbol $C_{\alpha\gamma}$ is used here for shear strains, instead of C_α which determines voids ratio changes in an oedometer, or $C_{\alpha\varepsilon}$ which determines volumetric strains. Here it is clear that γ_0 should be treated as the initial undrained shear strain developed by loading applied over some time period t_0.

Figure 6 demonstrated that undrained creep proceeded through the same mechanism as the original undrained embedment. If the mechanism remains unchanged, it must follow that shear strains γ will follow the same time law as settlements w. Therefore, eq. (12) can be rewritten for undrained creep settlements Δw_u

$$\frac{\Delta w}{w_0} = \frac{\Delta w_u}{w_u} = C^{u}_{\alpha w} \log_{10}\left(\frac{t}{t_0}\right) \tag{13}$$

where the original undrained settlement w_u is calculated at time t_0 when the load has just been fully applied. The undrained creep settlement rate $C^{u}_{\alpha w}$ in eq. (13) is identical to $C_{\alpha\gamma}$ in eq. (12).

Now Sheahan et al. (1996) showed that the stress–strain curves of overconsolidated clays tested undrained at different strain rates are almost indistinguishable when they are normalized by their appropriate peak strength. In the present work we use eq. (8) as the form of that relation. It is then possible to relate creep rate $C_{\alpha\gamma}$ to the strain-rate effect described by eq. (7). A method for translating between creep effects and strain rate effects was suggested by Lin and Wang (1998), for example. Here we will work the other way around, and also associate a tenfold increase of creep time with an average tenfold reduction of strain rate. The undrained strength c_u will be permitted to reduce with time in eq. (8) and Fig. 10, at a rate of 10% per factor 10 on time as suggested by eq. (7), and without altering either of the shape parameters b and $\gamma_{M=2}$. It is then easy to show (from eq. (8)) that, with $b = 0.6$, a 10% reduction in c_u causes a 19% increase in shear strain for any maintained shear stress inducing moderate strains (i.e., for $0.2 < \tau_{mob}/c_u < 0.8$). It should follow that $C^{u}_{\alpha w} = C_{\alpha\gamma} = 0.19$ for undrained creep in clays if the "10% per $\log_{10}t$" rule for rate effects is taken to be true.

Ultimately, of course, the clay drains by transient flow. As it will then be further from failure it is not surprising that that the rate of creep is seen to reduce. Furthermore, the deformation mechanism becomes more one-dimensional, although lateral strains do continue: compare Fig. 7 with Fig. 4 for test 3A. The ultimate drained creep slope $C^{d}_{\alpha w}$ can most conveniently be defined in a fashion analogous to eq. (13)

$$\frac{\Delta w_d}{w_u} = C^{d}_{\alpha w} \log_{10}\left(\frac{t}{t_c}\right) \tag{14}$$

where t_c is the time after which further effective stress changes due to consolidation are negligible. For test 3A this gives $C^{d}_{\alpha w} = 0.13$.

The transition between initial undrained creep and eventual drained creep is gradual. The creep slope $C_{\alpha w}$ in this case was simply taken to change in proportion to the degree of consolidation settlement. Figure 12 plots the data of settlement versus the logarithm of time for test 3A, with salient points and trend lines marked to demonstrate a back-analysis using eq. (7) for the rate correction of strength, eq. (8) for the undrained stress–strain relation, and with eqs. (13) and (14) for creep, as discussed.

At time t_0 in Fig. 12 the load has just been fully applied and the settlement $w_u = 0.82$ mm. By time t_1 a clear trend has emerged of w increasing linearly at a rate of 0.26 mm or 31% per factor 10 on t, which extrapolates back to a settlement of 0.84 mm at time t_0, perhaps suggesting that the elimination of 0.02 mm of clay unevenness at the foundation interface took 30 s to accomplish.

The settlement increment of 31% per factor 10 on time between t_1 and t_2 in Fig. 12 should be compared with 19% as predicted by the undrained creep relation of eq. (13). Note that an accompanying drop of 4% in excess pore pressures occurred at a depth of 0.55D during this interval, suggesting that the extra 12% per $\log_{10}t$ should be seen as the first signs of consolidation settlement. The solution by Senjuntichai and Sapsathiarn (2006) of transient flow below a rigid impermeable circular base, loading a deep poroelastic bed, similarly required 3 cycles of $\log_{10}t$ for its effective completion. Therefore, in accordance with eq. (1), the components $w_u = 0.82$ mm of immediate undrained settlement, $w_s = 0.44$ mm of creep settlement, and $w_c = 0.39$ mm of consolidation settlement have been marked on Fig. 12 at the end of loading in test 3A. This construction on the load response data of test 3A permits the back

Table 3. Foundation settlements and secant Poisson's ratio implied by creep and consolidation model.

Test label	D (mm)	w_t (mm)	w_u (mm)	w_c (mm)	w_s (mm)	$C_{\alpha w}^{u}$	$C_{\alpha w}^{d}$	ν'_{sec}
1A	50	3.20	1.94	0.61	0.65	0.19	0.07	0.34
2A	50	1.65	1.05	0.28	0.32	0.19	0.09	0.37
2B	100	1.64	0.91	0.32	0.41	0.19	0.13	0.32
3A	100	1.65	0.82	0.39	0.44	0.19	0.13	0.26
3B	50	1.64	1.11	0.27	0.26	0.19	0.09	0.38
3C	100	1.98	1.02	0.36	0.60	0.19	0.13	0.32

calculation of an effective Poisson's ratio $\nu' = 0.26$ from eq. (3), which is consistent with the data of Wroth (1975). Table 3 records similar quantities arising from the back analysis of the other tests. The variation in the implied value of ν' between 0.26 and 0.38 is not excessive, though it must be recalled that the secant value of ν' must be expected to vary with the magnitude of strain (and therefore the settlement to diameter ratio).

The variation in the observed drained settlement creep rate $C_{\alpha w}^{d}$ in the six tests, between 0.13 and 0.07, is more significant. It should first be noted that typical creep settlements in oedometer tests on clay conform to $C_{\alpha\varepsilon} \approx 0.02$ (see Mesri and Godlewski 1977), but there are two salient differences between $C_{\alpha w}^{d}$ and $C_{\alpha\varepsilon}$. First, the soil is not laterally confined beneath the foundation, so its settlement rate should be larger. Second, we have chosen to scale drained creep settlements with the initial undrained settlement, using eq. (14): if the drained creep mechanism were actually twice as deep as the undrained mechanism, the drained creep strains would result in double the drained creep settlements. Further centrifuge model testing would be useful in confirming creep mechanisms and corresponding settlement calculations.

The strategy adopted here for dealing with time related settlements is not conventional, but it is conveniently based on observed foundation settlements, rather than oedometer data that are generally applied by assuming an arbitrary elastic stress distribution. Both the consolidation settlements and the creep settlements are taken to be proportional to the initial undrained settlement.

Conclusions

The following conclusions can be drawn from this study:

1. Centrifuge model tests of circular foundations on the surface of overconsolidated clay beds have provided data of settlements with accompanying soil deformation mechanisms, over times ranging from 3 h to 7 years at the prototype scale. Pore pressure responses confirmed that the corresponding soil–foundation response ranged from fast undrained shearing with significant rate effects, through transient drainage with contemporaneous creep, to fully drained creep.
2. The method of preparation and testing of the clay models meant that their effective stress history was known. Furthermore, a suite of undrained triaxial compression tests had been conducted to relate the shear strength profile to stress history, and which validated a power curve as the stress–strain relation together with values of its key scaling parameter, the shear strain $\gamma_{M=2}$ required to mobilize half the shear strength. In a field application this could be replaced by a conventional program of coring and laboratory testing.
3. The back-analysis of undrained base penetration depended on making three adjustments to the measured soil strengths: a rate effect of 10% per factor 10 on strain rate or test duration; an anisotropy effect by which it was proposed that the operational strength in bearing was 0.77 times the strength in a triaxial compression test; and a large deformation correction that allowed for soil softening by at least 30% when proportional settlements w/D exceeded 15%, and which accounted for the corresponding overburden pressure in calculating net bearing pressures. Each of these assumptions was recognized to be a simplification of reality, but bearing capacity and settlement were then predicted with reasonable accuracy.
4. The successful prediction of ultimate consolidation settlements w_c following transient flow was based first on the ability to predict undrained settlement w_u, and then on the empirical use of elasticity theory to give $w_c/w_u = 1 - 2\nu'$ with a secant Poisson's ratio $\nu' \approx 0.3$. The time during which significant transient flow takes place covers a factor of 1000, which is much longer than with an oedometer. This is because of the influence of local drainage beneath the edge of a foundation, which creates additional settlement and load redistribution at an early stage.
5. Undrained creep was seen to follow the same mechanism as the initial undrained embedment. Creep settlements w_s before and during initial consolidation in these centrifuge tests were fitted simply by extrapolating from the undrained embedment, increasing at 19% per factor 10 on time. This creep settlement factor was obtained by combining the power law for stress versus strain with the commonly held proposition that strength should reduce by 10% per factor 10 on time. When wide surcharges are to be placed over deep clays, or when any loads are to be applied quickly in comparison with consolidation times, undrained creep and rate effects could and should be determined from site specific tests, such as triaxial tests carried out on high-quality cores. Fully drained creep was seen to adopt a different mechanism in the centrifuge tests, with settlement proceeding at a slower rate as the soil was further from failure. Further research on three-dimensional creep would be helpful.
6. The key to predicting foundation behaviour by this route is a good initial prediction of its undrained penetration, accounting for soil nonlinearity by the MSD method. The ultimate total settlements of the foundations tested here correspond to values of w_t/D between 6.4% and 1.6%, at factors of safety between 1.3 and 4.0, respectively, a reduction of proportional settlement by a factor of 4 accompanying a threefold increase in safety factor. It would, of course, be wrong to infer from this that the soil response was almost linear. The relationship derives from a variety of effects including the stress–strain relation being a power curve, the representative depth increasing with foundation width while with the soil strength also increases with depth and the stress–strain relation becomes stiffer as $\gamma_{M=2}$ reduces with reducing overconsolidation ratio.

Acknowledgements

The first author would like to thank Cambridge Australia Trust (Poynton Scholarship) and the Principals of UK Universities (Overseas Research Students Awards Scheme) for the financial support he received throughout his studies at the University of Cambridge.

References

Baracos, A. 1957. The foundation failure of the Transcona grain elevator. Engineering Journal, **40**(7): 973–977. [Reprinted by National Research Council of Canada, Division of Building Research, Research Paper no. 42.]

Cox, A.D., Eason, G., and Hopkins, H.G. 1961. Axially symmetric plastic deformations in soils. Philosophical Transactions of the Royal Society of London A: Mathematical, Physical and Engineering Sciences, **254**(1036): 1–45. doi:10.1098/rsta.1961.0011.

Davis, R.O., and Selvadurai, A.P.S. 1996. Elasticity and geomechanics. Cambridge University Press.

D'Orazio, T.B., and Duncan, J.M. 1987. Differential settlements in steel tanks. Journal of Geotechnical Engineering Division, ASCE, **113**(9): 967–983. doi:10.1061/(ASCE)0733-9410(1987)113:9(967).

D'Orazio, T.B., Duncan, J.M., and Bell, R.A. 1989. Distortion of steel tanks due to settlement of their walls. Journal of Geotechnical Engineering Division, ASCE, **115**(6): 871–890. doi:10.1061/(ASCE)0733-9410(1989)115:6(871).

Eason, G., and Shield, R.T. 1960. The plastic indentation of a semi-infinite solid by a perfectly rough circular punch. Journal of Applied Mathematics and Physics (ZAMP), **11**: 33–43. doi:10.1007/BF01591800.

Foott, R., and Ladd, C.C. 1981. Undrained settlement of plastic and organic clays. Journal of the Geotechnical Engineering Division, ASCE, **107**(8): 1079–1094.

Gasparre, A. 2005. Advanced laboratory characterisation of London clay. Ph.D. thesis, Imperial College of Science and Technology, London.

Horikoshi, K., and Randolph, M.F. 1997. On the definition of raft-soil stiffness ratio for rectangular rafts. Géotechnique, **47**(5): 1055–1061. doi:10.1680/geot.1997.47.5.1055.

Kulhawy, F.H., and Mayne, P.W. 1990. Manual on estimating soil properties for foundation design. Report No. EL-6800. Electric Power Research Institute, Palo Alto, Calif.

Kwok, C.-Y., and Bolton, M.D. 2010. DEM simulations of thermally activated creep in soils. Géotechnique, **60**(6): 425–433. doi:10.1680/geot.2010.60.6.425.

Ladd, C., Foott, R., Ishihara, K., Schlosser, F., and Poulos, H.G. 1977. Stress-deformation and strength characteristics. *In* Proceedings of the 9th International Conference on Soil Mechanics and Foundation Engineering, Tokyo. Vol. 2, pp. 421-494.

Lehane, B.M. 2003. Vertically loaded shallow foundation on soft clayey silt. Proceedings of the Institution of Civil Engineers, Geotechnical Engineering, **156**(1): 17–26. doi:10.1680/geng.2003.156.1.17.

Lin, H.D., and Wang, C.C. 1998. Stress-strain-time function of clay. Journal of Geotechnical and Geoenvironmental Engineering, **124**(4): 289–296. doi:10.1061/(ASCE)1090-0241(1998)124:4(289).

Mandel, J. 1953. Consolidation des sols (étude mathématique). Géotechnique, **3**(7): 287–299. doi:10.1680/geot.1953.3.7.287.

McMahon, B.T. 2012. Deformation mechanisms beneath shallow foundations. Ph.D. thesis, University of Cambridge.

McMahon, B.T., and Bolton, M.D. 2011. Experimentally observed settlements beneath shallow foundations on sand. *In* Proceedings, 15th European Conference on Soil Mechanics and Geotechnical Engineering, Athens, 12–15 September 2011.

McMahon, B.T., Haigh, S.K., and Bolton, M.D. 2013. Cavity expansion model for the bearing capacity and settlement of circular shallow foundations on clay. Géotechnique, **63**(9): 746–752. doi:10.1680/geot.12.P.061.

Mesri, G., and Godlewski, P.M. 1977. Time and stress compressibility interrelationships. Journal of the Geotechnical Engineering Division, ASCE, **103**(5): 417–430.

Osman, A.S., and Bolton, M.D. 2005. Simple plasticity-based prediction of the undrained settlement of shallow circular foundations on clay. Géotechnique, **55**(6): 435–447. doi:10.1680/geot.2005.55.6.435.

Prandtl, L. 1921. Über die Eindringungsfestigkeit plastischer Baustoffe und die Festigkeit von Schneiden. Zeitschrift fur angewandte Mathematik und Mechanik, **1**(1): 15–20. doi:10.1002/zamm.19210010102. [In German.].

Rosenberg, P., and Journeaux, N.L. 1982. Settlement limitations for cylindrical steel storage tanks. Canadian Geotechnical Journal, **19**(3): 232–238. doi:10.1139/t82-030.

Schiffman, R.L., Chen, A.T.-F., and Jordan, J.C. 1969. An analysis of consolidation theories. Journal of the Soil Mechanics and Foundations Division, ASCE, **95**(1): 285–312.

Senjuntichai, T., and Sapsathiarn, Y. 2006. Time-dependent response of circular plate in multi-layered poroelastic medium. Computers and Geotechnics, **33**(3): 155–166. doi:10.1016/j.compgeo.2006.03.005.

Sheahan, T.C., Ladd, C.C., and Germaine, J.T. 1996. Rate-dependent undrained shear behavior of saturated clay. Journal of Geotechnical Engineering, **122**(2): 99–108. doi:10.1061/(ASCE)0733-9410(1996)122:2(99).

Skempton, A.W., and Bjerrum, L. 1957. A contribution to the settlement analysis of foundations on clay. Géotechnique, **7**(4): 168–178. doi:10.1680/geot.1957.7.4.168.

Terzaghi, K. 1943. Theoretical soil mechanics. John Wiley and Sons, New York.

Vardanega, P.J., and Bolton, M.D. 2011. Strength mobilization in clays and silts. Canadian Geotechnical Journal, **48**(10): 1485–1503. doi:10.1139/t11-052.

Vardanega, P.J., and Bolton, M.D. 2012. Corrigendum: Strength mobilization in clays and silts. Canadian Geotechnical Journal, **49**(5): 631. doi:10.1139/t2012-023.

Vardanega, P.J., Lau, B.H., Lam, S.Y., Haigh, S.K., Madabhushi, S.P.G., and Bolton, M.D. 2012. Laboratory measurement of strength mobilisation in kaolin: link to stress history. Géotechnique Letters, **2**: 9–15. doi:10.1680/geolett.12.00003.

White, D.J., Take, W.A., and Bolton, M.D. 2003. Soil deformation measurement using particle image velocimetry (PIV) and photogrammetry. Géotechnique, **53**(7): 619–631. doi:10.1680/geot.2003.53.7.619.

White, D.J., Gaudin, C., Boylan, N., and Zhou, H. 2010. Interpretation of T-bar penetrometer tests at shallow embedment and in very soft soils. Canadian Geotechnical Journal, **47**(2): 218–229. doi:10.1139/T09-096.

Wroth, C.P. 1975. In-situ measurement of initial stresses and deformation characteristics. *In* Proceedings of the ASCE Specialty Conference on In-Situ Measurement of Soil Properties, Raleigh. Vol. 2, pp. 180–230.

List of symbols

A_f	foundation area
b	empirical exponent
$C_{\alpha\gamma}$	strain creep rate
$C_{\alpha\varepsilon}$	secondary compression index
$C_{\alpha w}^{d}$	drained creep settlement rate
$C_{\alpha w}^{u}$	undrained creep settlement rate
c_u	undrained shear strength
$c_{u,0}$	initial undrained shear strength
$c_{u,mod}$	modified undrained shear strength
D	foundation diameter
G	shear modulus
g	acceleration due to Earth's gravity
K_0	coefficient of earth pressure at rest
L	breadth of package (Fig. 1); load cell reading (Fig. 8*a*)
M_c	compatibility factor
m_f	mass of foundation
N_c	bearing capacity factor
n	acceleration factor in centrifuge
OCR	overconsolidation ratio
q	foundation pressure
q_{ult}	bearing capacity
t	time
t_0	duration of initial loading phase
t_c	time after which further effective stress changes due to consolidation are negligible
u	pore pressure
u_{static}	static pore pressure
W	width
w	settlement
w_t	total settlement
w_u, w_c, w_s	immediate, consolidation, and secondary components of settlements respectively
$w_{u,exp}$	experimental undrained settlement
$w_{u,pred}$	predicted undrained settlement
Δw_d	increment of drained creep
z	characteristic depth
α	creep parameter
γ	shear strain
$\dot{\gamma}$	shear strain rate
$\dot{\gamma}_0$	initial shear strain rate
$\gamma_{M=2}$	mobilization strain
Λ	empirical exponent
$\sigma'_{v,0}$	in situ vertical effective stress
$\sigma'_{v,max}$	preconsolidation stress
τ_{mob}	mobilized shear stress
ν	Poisson's ratio
ν', ν'_{imp}	effective and implied effective Poisson's ratio, respectively
ν'_{hh}, ν'_{vh}	effective Poisson's ratios for horizontal and vertical loading, respectively
ν'_{sec}	effective secant Poisson's ratio
ν_u	undrained Poisson's ratio